HEAVY-ION COLLISIONS

William J. WILLIS,
CERN, Geneva, Switzerland

1. INTRODUCTION

1.1 States of the Vacuum

There is powerful evidence for the existence of quarks and gluons from scattering experiments involving nucleons, pions and other hadrons. It is widely accepted that the failure to observe free quarks is due to the very large energy which would be necessary to place such a particle in the physical vacuum, the ordinary vacuum found in the laboratory [1]. An attempt to draw a free quark into the vacuum then creates particle-antiparticle pairs so that the net colour quantum number remains zero, and only the ordinary hadrons remain. This picture is supported by attempts to evaluate the states of quantum chromodynamics (QCD) numerically, but reliable results are so far difficult to obtain. The origin of this effect is the highly complicated but ordered states of virtual excitations of the physical vacuum in QCD, analogous to vacuum polarization in quantum electrodynamics, but so strong in this theory as to produce a qualitative change in the physical vacuum from the simple empty state of a world with very weak interactions.

Furthermore, the theory indicates that this ordered state of the physical vacuum can be destroyed by the presence of a sufficient density of quarks or gluons, reverting to a state better described as a simple vacuum, usually referred to as the 'perturbative vacuum', with quarks and gluons moving freely, except for their mutual interactions. This high density of particles, or equivalently a high energy density, must be present for a sufficiently long time for this change in the vacuum to develop.

Since the energy density in our universe was high at short times after its formation, the universe should have retained the perturbative vacuum up to times of about 10^{-6} seconds, then completing a transition to the physical vacuum containing a gas of hadrons at around 10^{-5} seconds. The hadrons condensed to nuclei at a much later time. This phase transition can have important consequences for the limit on the allowed baryon density in the Universe, and thereby on the question of "dark matter" [2]: it can be that the density fluctuation associated with a first order QCD phase transition changes the nucleosynthesis in the universe in such a way as to require no dark matter!

The Physics described above has little direct experimental support. The direct tests of QCD are at high energies, where the confinement effects play no direct role, being handled phenomenologically as "hadronization". It is almost universally accepted that the structure of QCD is so well defined that there is little doubt that the above picture is correct, and that experimental

verification is desirable but not of the very highest priority. Perhaps a different viewpoint is more interesting: to note that the physics described in a kind of condensed matter physics, but dealing with quarks and gluons rather than molecules. It is characteristic of the condensed matter physics of a strongly interacting, non-perturbative system to reveal phenomena which were *completely unanticipated. Often these phenomena are interesting and even important to science*, though they may tell us nothing we did not already know about the underlying basic interactions. It may even be that we have already found such an example in the discoveries presented in Chapter 5.

The experiments relevant to the physical vacuum fall into two distinct categories: those relating to deconfinement at high energy densities and those seeking evidence of the specific response of the physical vacuum to colour excitations, and these are dealt with separately in the following sections.

1.2 High Energy Density Phenomena

1.2.1 Successive States of the Vacuum

Here we will describe in a little more detail the successives states through which our universe is claimed to have passed, and which we hope we can produce in a laboratory. We must deal with volumes which are sufficiently extended and long-lived to be described as fluids with well defined properties. We then expect to find at least three different fluids in successive stages of expansion of a high energy density state. This is shown in Fig. 1 as snap shots of a small region at different times. At the highest density we see the gas of deconfined quarks and gluons known to be predicted by QCD in very high energy density conditions. Since these particles carry colour charge, we may describe it as a plasma, the quark-gluon plasma (QGP). Although there are none of the usual hadrons present, there could still be excitations corresponding to clusters of quarks and gluons carrying the quantum numbers of hadrons. At the other extreme, at low energy density, we see a gas of hadrons, of mesons and baryons. This gas is a system whose properties can presumably be predicted reliably at low density, since we know the low energy scattering amplitudes experimentally.

In terms of QCD, this gas of hadrons consists of quarks grouped in colourless combinations, maintained by the confinement mechanism of the physical vacuum described earlier. A phenomenological picture of this confinement which allows one to draw an easily understandable picture, is the bag model. In this model the quarks are confined to small cavities in the physical vacuum which contain the perturbative vacuum, the bags. In this picture the hadron gas consists of the physical vacuum with a small fraction of its volume occupied by the bags containing quarks. When this phenomenology is used to explain the observed distributions of hadron masses, one concludes that there is a large energy associated with the creation of a bag. In the states of thermal-equilibrium

shown in Fig. 1, this bag energy is equivalent to a large latent heat needed to go from the state with a physical vacuum to that with the perturbative vacuum. A mixed phase will necessarily arise in the cooling of the quark gluon plasma in this case, which will contain both deconfined quarks and hadrons. To draw a picture of this state requires much more knowledge than we possess at the present time, but the ingredients it must contain are shown in Fig. 2. Here we see different regions of physical vacuum imbedded in the original perturbative vacuum. Inside these regions we see bags, corresponding to hadrons. In the regions of perturbative vacuum which are simultaneously present, we see quarks and gluons which are not confined but still have strong mutual interactions. If the phase transition has indeed a large heat, it is a first order transition and the phases must be spatially separated as shown. We can only speculate about the characteristic size of these regions and the nature of their boundaries. We note that the temperature of this state is held constant by the latent heat of the confinement transition while it expands.

1.2.2 Collision of the High Energy State in the Laboratory

There may be signs of the transition between the two vacuum states in the early period of universe, still existing today [2], but we are interested in investigations in the laboratory. The only way to achieve the energy densities required, that is comparable to the energy density of a hadron, of order 1 GeV/fermi^3, is in the collisions of high energy particles or nuclei. Our strategy is to find suitable high energy collisions which provide a high energy density over a sufficiently large volume in order to obtain the needed thermal equilibrium and long lifetime. For a given accelerator, it seems clear that we will gain in this respect by colliding nuclei rather than hadrons. These considerations have led to programmes of physics with nuclear beams at the CERN SPS and the Brookhaven AGS [3].

The techniques of equilibrium thermodynamics demand systems large compared to the scattering length of the constituents. Because of our inability to calculate in non-perturbative QCD, we do not know the interaction length of the soft constituents and consequently we cannot say how large a system is required. This must be determined from experiment, using arguments described in the next section, where we will find that high energy collisions of hadrons certainly show some signs of thermal equilibrium, but equally certainly are not fully in thermal equilibrium. This can lead us to hope that a relatively small increase in the size of the projectiles, for example moving from one to tens of nucleons, might be sufficient to attain our goal.

An element of pessimism was present in the early consideration of whether the initial collisions between two nuclei would adequately transfer energy into a system not too far from thermal equilibrium. This concern reflected a knowledge that as hadron energy increased the absorption of the energy in the nuclear target became less complete.

An object of initial experiments is to show how efficient high energy projectiles are in creating the desired states. The measurements related to energy deposition are relatively straightforward and have allowed results to be obtained in a short space of time.

1.2.3 Measurements Sensitive to the Evolution of High Energy Density States

The observables which are sensitive to the nature of the state produced are difficult to measure and the results of the recent experiments are not yet complete in this respect. In these lectures I shall emphasize the simpler observables such as the transverse momentum and angular distribution of different particle types and the information on the space time structure which can be obtained by studying the intensity interferometry by correlations of two identical particles. In principle these measurements are sensitive to the collective expansion of the system, and can measure the spatial distribution of the matter at the time the pions are formed, and the length of time over which they are emitted. This can, in turn, give us information on earlier stages in the evolution of the matter. I shall not discuss the important questions of the thermal radiation of photons, or virtual photons appearing as pairs of leptons, or of the effect of the environment on the production of bound states of quarks, such as the heavy vector resonances.

1.3 Response of the Vacuum to Soft Excitations

The previous section describes attempts to destroy the order of the physical vacuum and cause the transition to the perturbative vacuum by increasing the temperature or quark density of the environment. On the other hand many of the most characteristic and interesting condensed matter phenomena occur at low temperature. In this section, we turn our attention to the possibilities for investigating the response of the physical vacuum in its normal, cold, environment.

We might think of doing that by the precision spectrometry of quark-antiquark states, such as the J/ψ. Unfortunately, it has been found that the energy levels of the observable spectrum are not very sensitive to these questions [4]; in essence, as the energy of two quarks is increased, the continuum arrives before the states are sensitive to the details of the vacuum outside the bag. Use of hadron scattering for this purpose seems even less likely to succeed. We know that the hadrons and hadron resonances can be described to a good approximation as elementary, colourless objects, so that their excitations of colour modes in the vacuum must be very weak.

These considerations show us that we must search for experiments where free colour is exposed in the interaction, and then look for probes which are somehow distinguishable from the complexities of ordinary hadron interactions. The prototype of a reaction where their colour is certainly present is the production of quark-antiquark pairs by the annihilation of e+e-, Fig. 3(a), the quark and antiquark carry opposite signs of colour. The quarks evolve into a cascade of quarks and gluons in the process of

hadronization, for which there is no real theory, and the colour is gradually neutralized as hadrons are formed. For some time, until this neutralization has taken place, the physical vacuum is exposed to colour excitation multipoles around the creation point of the quark-antiquark pair. We could imagine selecting events where there were no hadrons along a specific segment of the quark path thereby *selecting events with a certain degree of coherent colour excitation. Somewhat less clean, but* equivalent, colour excitation must be present in any high energy interaction which generates the quark gluon cascade and hadronization, in distinction from diffractive reactions that merely excite hadron resonances.

Given the availability of colour excitation, where can we find distinctive probes? The first thing to notice is that the effects we seek must necessarily be those with wavelengths larger than the size of the bag, of order one fermi, because there is no physical vacuum inside that volume. This argument can be reversed, there are no conventional hadronic effects with wavelengths larger than the size of hadrons, except for the decay of long-lived resonances, a process which can be taken into account. It seems clear then that we must seek effects which have wavelengths which would be considered anomalously long for ordinary hadronic interactions. The most obvious and probably the cleanest probe is the radiation of direct photons with wavelengths greater than one fermi or so. In this case we have the advantage that the background from hadronic interactions indicated in Figs. 3(b) and 3(c), can be calculated with some precision.

Investigations on these lines will be reported in a later chapter and indeed some interesting effects have appeared.

2. ENERGY DEPOSITION

2.1 Introduction

The experimental study of energy deposition is the first task in the study of high energy density. It is also a subject of interest in that it allows us to learn something about the space time evolution of high energy particle systems which have interacted one or more times. This can be studied already with hadron-nucleus collisions, whereas in the nucleus-nucleus collisions we can study the space-time evolution of more complex configurations which have already been disturbed by the previous collisions. Since there are phenomenological models for these subjects but no real theory, the information we obtain is of basic interest.

2.2 Kinematics and Geometry

Already from the experiments on proton-proton interactions, we see most of the physical features which will be important in the more complex reactions. The first of these is that despite a very wide fluctuation from event to event, there is a strong tendency for a major fraction of the incident

energy to be retained by a single baryon in the final state. This indicates a tendency for the incident nucleon to retain its identity and a good fraction of its energy, as the "leading baryon". The rest of the energy is carried by a relatively large number of particles, usually pions. The situation is then qualitatively the same as that for an electron losing energy by bremsstrahlung, which forms a useful *simple picture. Consider an electron* which enters an absorber with a unique energy. As it traverses the absorber, its average energy falls and it develops a spread in energy due to the fluctuations in energy loss. After about 0.7 radiation length, its energy distribution is approximately uniform from the initial energy down to zero. Deeper in the absorber, the energy distribution peaks at zero with an asymmetric tail toward higher energies. After a proton-proton collision, the energy spectrum of the leading baryon resembles that of an electron which has traversed about half a radiation length. This analogy remains useful when the target is a nucleus rather than a proton, corresponding to a thicker absorber. The baryon distributions then peak well below half of the initial value, for a heavy target nucleus.

2.3 Kinematics

If the incident energy is very high, the average energy of the leading baryon can still be quite relativistic even if it has lost a major fraction of the incident energy. For this reason it is more convenient to use a different variable to describe its energy distribution. The variable most suited for this situation is the rapidity variable defined by

$$y = \frac{1}{2} \log \left(\frac{E + P_z}{E - P_z} \right)$$

It is seen that y is a logarithmic energy variable, and has the property that the shape of distributions in this variable are invariant under Lorentz transformations along the beam axis, z.

To illustrate its use we show in Fig. 4(b) the y distribution of an electron after 0.5, 1. and 1.5 radiation lengths compared with the energy distributions in Fig. 4(a). It is seen that the shape of the y distributions is not changing as drastically as in the energy variable, as the absorber thickness is changed. The energy loss of the electron can be described by a shift Δy between the rapidity of the incident electron and the peak of the degraded electron distribution.

The energy which is lost by the incident baryon reappears mainly in the form of many "soft" mesons (i.e. with energies small compared to the beam), mostly pions. It is convenient to describe the many particles produced by a global variable which is directly measurable and closely related to the energy density produced, the "transverse energy" defined by

$$E_T = \sum_i E_i \sin\theta_i$$

where i is summed over all particles. This quantity can be measured directly by a "calorimeter" or total absorption counter, which absorbs all the energy of each particle and provides a signal proportion to its "available energy". The calorimeter must be segmented into many small elements, each characterized by

polar angle θ_i (and usually the azimuthal angle ϕ). The elements may then be summed with weights $\sin\theta_i$, and if its output is linear, the sum over particles is achieved automatically. This technique works no matter how large the number of particles in the interaction may be. The measurement yields the "energy flow" in two dimensions. More convenient than θ and ϕ are η and ϕ, where η is the "pseudorapidity", a logarithmic angle variable.

$$\eta = \frac{1}{2} \log \frac{1 + \cos\theta}{1 - \cos\theta} = - \log \tan \theta/2$$

Note that for $p_T >> m$, $\eta = y$, explaining why it is a most convenient variable, though since the peak of the p_T distribution of the produced particles is near m, care must be exercised in its use.

2.4 Formation Zone

It is natural to ask why the emphasis is put on the energy loss of the leading particle: should not the produced particles also lose energy as they traverse a large nucleus? After all, we are familiar with the development of a cascade shower when an electron traverses an absorber, but is precisely in the case of the electromagnetic cascades that it was pointed out that the energy loss of the produced particles is suppressed at sufficiently high energies: the formation zone effect of Landau, Migdal and Pomeranchuk. From uncertainty principle arguments it is clear that for sufficiently large Lorentz time dilations, the time Δt between the successive collisions between target particles is less than the time $\Delta E/\hbar$ required for the produced particles, characterized by some appropriate energy ΔE in the rest frame of the incident particle, to manifest themselves as distinct entities.

This leads to a suppression of cascading at large incident energies. In the case of hadronic collisions, it is major effect throughout the energy region of interest, since ΔE must be of the order of m_π, and m_π/hc is comparable to the spacing between target nuclei. It becomes important for electromagnetic cascades above present accelerator energies, however.

The effect is illustrated in Fig. 5 [5], which compares the distribution of charged particle multiplicity for hydrogen and lead targets. For the high energy half of the rapidity range, the collisions with lead show no higher multiplicity than those with protons, while a cascading of secondaries would have increased the multiplicity.

2.5 Fate of Deposited Energy

2.5.1. Several very simple pictures have long been used to provide a basis for understanding the gross feature of the produced particles, especially their energy and number flow. Although this is properly a dynamical question, these simple models emphasize a kinematic picture, appropriate for different cases. They can be described as kinematic hydrodynamic models, to distinguish them from real hydrodynamical

calculations which include phase changes between different states, accurate description of the meson gas, and so on. They are useful for a qualitative interpretation of data described by global variables.

2.5.2. The Fermi Model

Here some fraction of the initial centre-of-mass energy is transferred to a system which can be described as a fluid which dissipates isotropically, in some combination of radial expansion and thermal motion [6]. In the pseudorapidity approximation, the distribution of transverse energy flow is then

$$\frac{dE_T}{d_\eta} = (\text{hyperbolic}\cos(\eta))^3$$

It was long ago discovered that this model does not describe the particle production in hadron-hadron collisions at any energy.

2.5.3. The "Shuryak-Bjorken Model"

A free expansion at velocity c along the beam direction, appropriate for very high energy where the produced particles are distributed over many units of rapidity, while the average transverse momentum, p_T, is small and independent of rapidity [7]. Both dN/dy and $dE_T/d\eta$ are constant in this model, while $dN/d\eta$ has a dip of kinematic origin. The distribution of particles produced in $p\bar{p}$ collisions at centre-of-mass energies of 540 GeV fits these distributions, as is predicted by the multiperipheral model of hadron interactions at very high energies.

2.54. The "Landau Model"

The deposited energy is left in a disc, with dimension along the beam small compared to the transverse dimensions [8]. This disc then expands longitudinally, at a rate large compared to the transverse expansion, in such a way that the p_T of the particles observed in different rapidity regions is the same. The dN/dy or $dE_T/d\eta$ is a Gaussian. It describes well the nucleon-nucleon data at centre of mass energies up to 63 GeV. The previous two models represent approximate limiting cases of this one, at low and high energies.

2.6 Energy Deposition by protons

We examine first data on "stopping", the rapidity shift between the incident proton and the leading proton exiting from the collision, ΔY. The comparison between proton-proton and proton-lead collisions is shown in Fig. 6 in terms of ΔY [9]. There is indeed much more energy lost in traversing the lead nucleus. In interpreting this figure, it must be remembered that geometry plays an important role in the hadron collisions with a heavy target, as we learn immediately by the fact that the total cross-

sections vary as $(A_{TAR})^{2/3}$ If we treat the target as a sphere containing A nucleons, and ask the mean number of collisions a proton will make with the nucleons in the target, $\bar{\nu}$, assuming it travels always along the incident direction, a geometrical calculation leads to $\bar{\nu} = A\sigma_{pp}/\sigma_{pA}$, and for lead $\bar{\nu} = 2.7$. It is clear that many of the p-A interactions correspond to collisions with the outer part of the nucleus, where ν is closer to one, so that the central collisions, where $\nu > 3$, must have larger energy losses than in the average represented in Fig. 6, leading to the two bands shown. The conclusion is that a central collision with a lead nucleus takes away on the average considerably more than half the energy of a proton. This energy appears in the form of produced particles, as shown in Fig. 7 [10], showing E_T integrated over rapidity, for proton-lead collisions. A feature of this curve is that it extends far beyond the kinematic limit for E_T produced in p-p collisions, showing the importance of collisions with many target nucleons. Superposition of independent nucleon-nucleon collisions can reproduce many features of the data, but not all, for example the $dE_T/d\eta$ distributions as shown in Fig. 8 [10]. Important cascading of the produced particles in the target must be present, showing that it is not much suppressed by the "formation zone" effect.

2.7 Nucleus-Nucleus collisions

Here the gross features of the collisions are even more fixed by the geometry. Consider the interactions of nuclei with matter density given by the charge density measured in electron scattering. Now compute the distribution of the number of nucleon-nucleon collisions by convoluting the two nuclear density distributions for random geometries, and using the free nucleon-nucleon cross-section, to yield Fig. 9 [11]. The collisions with few interactions correspond to a grazing geometry of the two nuceli collisions, and the abrupt drop for high numbers of collisions corresponds to the case with the central axes of the nuclei aligned so that the maximum number of nucleon-nucleon collisions geometrically possible has been achieved. The unusual flat portion of the curve is just a property of the geometry.

The data on E_T, Fig. 10 [12], show an obvious resemblance to the geometrical convolution indicating that a geometrical superposition of nucleon-nucleon collisions will explain the general features of the data. The $dE_T/d\eta$ distribution seen in Fig. 11 [12] shows that at 200 GeV/nucleon, we are far from the ultra-high energies which would give a flat plateau. In fact, the data fit the Gaussian of the Landau model, with a width only about twice as wide as that of the extreme limit of the Fermi model. This will have important consequences in the next section.

2.8 Energy Density

The purpose of the nucleus-nucleus collisions was to reach high energy densities, ε. Measurement of the true energy densities achieved will require subtle measurements, but rough estimates may be attempted from the global variable $dE/d\eta$. Bjorken [7] pointed out that in the conditions of the model of 2.5.3, one can compute a scaling of the energy density

$$\varepsilon = \frac{1}{\pi R_{BEAM}^2 \tau_0} \frac{dE_T}{d\eta}$$

with τ_0 an unknown constant, usually taken on dimensional grounds to be one fermi/c. If we follow this practise, we may insert the largest values of $dE_T/d\eta$ obtained in the data corresponding to sulphur-uranium in Figs. 10 and 11, $dE_T/d\eta$ = 140 GeV and obtain $\varepsilon = 3$ GeV/fermi^3.

Aside from the lack of knowledge of the value of τ_0, this estimate suffers from the obvious disagreement of the model with the shape of $dE_T/d\eta$, a narrow Gaussian instead of a wide plateau. Anticipating the result of 3.1, that the p_T of the produced particles is independent of y, at least for 200 GeV/nucleon beams, we see that it is appropriate to use at least the kinematics of the Landau model (the dynamical aspect is irrelevant here). In this way, it has been found that the observed highest values of $dE_T/d\eta$ correspond to essentially all the energy of the incident beam being deposited in a Landau "fireball". Since the energy is then known, one can try to compute ε by an estimate of the fireball volume on geometrical grounds. Its transverse size is just the area of the smaller nucleus. The longitudinal extent requires a dynamical assumption. If indeed full stopping has been achieved in the most extreme collisions, it seems correct to assume it has been Lorenz contracted as in the Landau model proper. The ε obtained could be as high as10 GeV/(fermi)^3 [13]. Either of these estimates is large compared with the energy density of a hadron, justifying the hopes that the high energy nuclear collisions would reach a new regime of energy densities. To investigate whether the equilibrium implied by such a large energy has indeed been achieved, we must proceed to study more detailed observables.

3. SPECTRA OF CHARGED MESONS

3.1 Transverse Momentum

In the previous chapter, we considered the most global description of high energy collisions, the energy flow, and showed that interesting physics can be gleaned from it. The next step is to study the ensemble of particles which carry away the energy deposited. At high energies, these are mostly mesons, pions and kaons. We often characterize them by their "Lorentz invariant inclusive cross-sections"

$$E\frac{d^3\sigma}{d_3p} = \frac{d^3\sigma}{dyd^2p_T}$$

In high energy proton-proton collisions, as well as in low energy nucleus-nucleus collisions, the data show a greater regularity when plotted against $m_T = (p_T^2 + m^2)^{1/2}$ rather than p_T. We show this in Figs. 12 [14] and 13 [15]. We see that the curves are good fits to exponentials when using m_T, and even with the same slope in the case of the p-p collisions, whereas there is a distortion for $p_T < m$, essentially due to a phase space factor, where p_T is the variable. This good fit to an exponential has a natural explanation, in that a thermal distribution has just this form in these variables. We see at

higher m_T, the cross-section for high energy p-p collisions become flatter, approaching a power law behaviour expected for the hard scattering of individual quarks, a regime we shall not discuss.

It is not at all certain to which degree the ensemble of particles is really thermal, and further, in most of the cases discussed below, there is not a simple exponential even in the low m_T region. We shall not speak of temperatures, but of the slope of the distribution, between defined limits. This would be proportional to 1/T in the truly thermal case.

3.2 Collective flow

It will be noticed that the slopes for pions and protons are different in Fig. 13 but the same in Fig. 12. The difference in the case of nuclear collisions is known to be due to a collective outward flow of the hot matter produced in the collision. This is inevitable in the expansion of a hot system into vacuum. The change in the distribution due to giving a thermal distribution a fixed radial Lorentz boost, with a velocity of v_c, has been calculated by Siemens and Rasmussen [15]. For a massless particle, the effect is just to increase the inverse slope, T_{eff}, by a factor γ_c $(1-v_c)$ cos h (γ_c). For a massive particle, for an initial $T_i << m$, the effect is to produce a peak at the energy corresponding to the radial velocity v_c. A fit to pions and protons to Fig. 13 gives $v_c \approx 0.3c$, and the T_{eff} for pions from the inverse slope, 100 MeV, corresponds to a thermal $T_i = 30$ MeV. This is an instructive cautionary lesson on interpreting inverse slopes as temperature, but also is most illuminating in regard to the dynamics of the collision.

The fact that no difference in slope is seen between pions and protons produced in high energy p-p collisions is susceptible to two explanations. Often it is assumed that there is just not a system of sufficient size to produce the degree of equilibration necessary to give radial flow. Another possibility is that in this system the energy is carried by quarks and gluons which are not free to expand, due to the confining effect of the physical vacuum surrounding the collision. If this is the case, making the system larger will not lead to the appearance of radial motion. Since we *do* see radial motion at low energies, there would have to be some energy region where the radial motion disappeared, more or less sharply.

3.3 Results with nuclear targets and beams

Measurements of the negative particle (mostly pion) spectra from proton and nuclear beams on a W target are shown in Fig. 14 [16]. The proton-proton results are shown as curves with arbitrary normalization. The difference between the nuclear target data and the p-p spectrum is similar for the different beams. We may say that the slope is the same as in p-p for the region around $p_T \approx 300$ MeV/c, where the majority of the pions are found, with a region of steeper slope for $p_T \approx 100$ MeV/c, and a flatter slope at high p_T. The latter, "Cronin effect" [17] is usually assumed to be a hard parton scattering phenomenon related to multiple quark interactions and the modified nuclear structure function inside the nucleus. In Fig. 15, the ratio of the spectra for the different beam particles is shown

to display better the small differences in the spectra. We see that the changes from p-p to p-w are enhanced for heavier projectiles, but the main conclusion is a substantial constancy in the mid-p_T range for a great variation of beam and target.

In Fig. 16, the dependence of the average p_T in the mid-region on the E_T measured in the associated event is shown [16]. Again the main impression is of a remarkable stability of the mid-p_T slope. The small increase noted is compatible with the change in the influence of the Cronin effect as the geometry of the collisions is changed by varying E_T: the more peripheral events should resemble p-p collisions.

A fit has been made to the pion p_T spectrum from oxygen collisions in the streamer chamber, with a model incorporating a more complex pattern of radial flow than a simple boost, superimposed on a thermal distribution [18]. The radial velocity is not a constant but depends on the square of the distance from the central point in the fireball, reaching v_c at the outer edge. The result is no longer an exponential but a curve which can fit the data, if v_c attains the rather large value of 0.78 as shown in Fig. 17. The streamer chamber has measured neutral strange particles as well, and in Fig. 18, their p_T spectrum is shown as well, with a fit to the radial expansion with the same velocity and temperature. The agreement is satisfactory.

The alert reader will have noticed that the curvature in the spectrum which is here fitted by the form of radial expansion is very similar to the Cronin effect in p-nucleus spectra which is usually interpreted as a hard scattering effect. There seem to be three possibilities. Either the Cronin effect is also really a radial expansion effect, or the close resemblance between the p-nucleus and oxygen-nucleus spectra is accidental, or the curvature is not really a radial flow effect.

3.4 Thermal and Flavour Equilibrium

In considering what conclusions to draw from these measurements, we draw attention to the arguments of E. Shuryak [19], who proceeds from examining the hypothesis that the particles produced in hadron-hadron collisions are far from thermal equilibrium. One would then expect as the size of the collision volume and the number of particles in it are increased, that there will be more collisions between particles in the final state, inevitably moving the particles toward thermal equilibrium. Since estimates show that the number of final state collisions in ^{16}O-W collisions should be considerably larger than in p-p collisions, on the hypothesis, we should then see a considerable change in the p_T mid-region unless the non-equilibrium hadron distribution and the thermal distribution were the same by coincidence. The precision of the constancy of the p_T slope with beam, target and E_T is such that such a coincidence seems unlikely, and thus we are tempted to conclude that the distribution in nucleon-nucleon collisions must be close to thermal.

This conclusion can be strengthened by independent evidence for the multiple interactions characteristic of a large system. Such evidence is available in the evolution of flavour with interaction volume [20]. The rate for production of strangeness and charm are relatively slow, so it is much more likely that thermal equilibrium will be achieved in nucleon-nucleon collisions than that the strangeness or charm will reach equilibrium values, since each collision alters momentum, but only a small fraction change strangeness. We may consequently expect to see strangeness enhancements even if no change in P_T slopes is seen. This is indeed the case: at AGS energies, where the K^+/π^+ increases from $\approx$ 5% proton collisions to 20% in ^{28}Si-Au collisions [21]. In the streamer chamber experiment on S-S collisions, a strong increase in the fraction of strange particles with accompanying multiplicity is seen, as shown in Fig. 19 [17]. Whether such an increase can be foreseen in a hadron gas, or requires the higher rates predicted in a deconfined state, involves models which need to be further constrained by other measurements, but the strong effect of rescattering, and the equilibration is unequivocal [20,22].

Similar remarks apply to the striking suppression of J/φ production. Whether or not this requires the properties of the deconfined state, it does imply the existence of a dense and sufficiently extended system [22].

The following chapter present further arguments to show that there are sufficient collisions to produce equilibrium and thereby collective flow phenomena, and that therefore constancy of P_T slope is a sign of a fundamental physics result and not a simple superposition of many nucleon-nucleon collisions.

4. PION INTERFEROMETRY

The use of second-order interferometry using intensities rather than amplitudes was suggested by Hanbury-Brown and Twiss [23]. The idea can be explained for two sources of monochromatic light, Fig. 20. The Bose-symmetry of the amplitude for two spin zero mesons of momentum $k\hbar c$ requires the amplitude of the form

$$A_{\gamma\gamma} = \exp [ik (R_{11} + R_{22})] + \exp [ik (R_{12} + R_{21})]$$

which, for small θ, gives

$$|A_{\gamma\gamma}|^2 = 1 + \cos (Lkq).$$

Evidently, the symmetry of the amplitude leads to an interference term in the intensity even though the phase is lost. Observation of the oscillatory term in the two photon correlation function allows one to measure θ. This is of course a mainstay of radio astronomy and has also been applied in the optical region.

The idea can be applied to measurements with identical hadrons, but the details become much more complicated [24]. The fact that the source is strongly time-dependent must be taken into account [25]. Coulomb and strong interactions corrections must be evaluated [26]. It turns out that, roughly

speaking, the behaviour of the correlation of the spatial component of the difference of two meson four-momenta gives the spatial dimensions of the source, while the energy difference gives the lifetime. Further consideration is required of coherent motions and the effect of long-lived resonances [27].

The difficulty with applying this method is that only a small fraction $\leq$1%, of all pion pairs fall close together in phase space, in the region where the correlation is important. Few experiments have had enough data to give accurate results, or to allow an investigation of the dependence of the correlation on other event parameters. In Fig. 21 we show the result with the largest statistics, a p-p experiment [28], in terms of the two pion correlation function

$$C(Q) = \frac{\frac{d^2\sigma_{12}}{dp_1\,dp_2}}{\frac{d\sigma_1}{dp_1}\,\frac{d\sigma_2}{dp_2}}$$

where $Q^2 = |p_1 - p_2|^2$ is the best single parameter to exhibit the correlation. We see the general features of all hadron results, a correlation for $Q \leq 300$ MeV, corresponding to a distance scale of order 1 fermi, with a maximum excess somewhat less than one unit. While the simple theory of the effect would predict a Gaussian shape, the observed shape indicates some more complex physics is involved, perhaps contributions from long-lived resonances, perhaps from some new element in "soft" physics. Note the large errors for the small Q bins, even with a sample of 10^6 pairs.

In the case of hadron interactions, no information has been extracted from multi-variable analyses which was not already implied in the C(Q) distribution. Geometry is more important for nuclear collisions, and one may hope to measure three variables [29]. One choice of variables is that shown in Fig. 22. The picture is drawn in a particular frame where, one pion is perpendicular to the beam axis. The second pion may then be along the beam, "longitudinal", along the direction of the first pion, "out", or the other direction in the transverse plane, "side". Hydrodynamic calculation shows that the ratio of the two transverse dimensions is sensitive to the passage of the system through a first order phase transition with a large latent heat. In that case, the system remains for a relatively long time in the mixed phase while the deconfined quarks assemble into hadrons. The R_{out}, which measures this time, can then be much larger than R_{SIDE}, which measures the transverse size of the system at "freeze-out" the last interaction of the pions.

The streamer chamber experiment has succeeded in the difficult task of measuring these correlations in the high multiplicity environment of ^{16}O-Au interactions, as shown in Fig. 23 [30]. The results are given in Table 4.1, for two different rapidity intervals, $2 < y < 3$, the region of the fireball, and $1 < y < 2$, which may be considered a control region. The quantity Λ measures the strength of the correlation: $\Lambda = 1$ corresponds to a Gaussian with $C(0) = 2$.

Table 4.1

Pion source parameters extracted from the streamer chamber analysis of the 200 GeV/n 0 + Au → ππ correlation data with separation of RT into R_T^{side} and R_T^{out}. Rapidity intervals at midrapidity (2 < y < 3) and backward of midrapidity (1 < z < 2) were analysed.

Rapidity Interval	Gaussian R_T(fm)	Gaussian R_L(fm)	Gaussian Λ
1 < y < 2	4.3 ± 0.6	2.6 ± 0.6	$0.34^{+0.09}_{-0.06}$
	R_T^{side} = 4.0 ± 1.0 fm	"	"
	R_T^{out} = 4.4 ± 1.0 fm	"	"
2 < Y < 3	8.1 ± 1.6	$5.6^{+1.2}_{-0.8}$	0.77 ± 0.19
	R_T^{side} = 6.6 ± 1.8 fm	"	"
	R_T^{out} = 11.2 ± 2.3 fm	"	"

The results are very suggestive. The dimensions in the control region are comparable to the geometrical size of ^{16}O, R = 3 fermi, but in the fireball region, large values are seen. The R_{out} is particularly large, which might optimistically be taken as a sign of the long-lived state predicted with a phase transition. Before reaching a firm conclusion, more information is needed particularly since it has been shown that somewhat similar results could be simulated by long-lived resonances. It will probably be essential to examine the correlations as a function of the p_T of the pions, as well as providing more information on the level of resonance production, particularly of the ρ and ω^o, which could partially simulate this effect [31].

5. SUMMARY OF CONCLUSIONS ON NUCLEUS-NUCLEUS COLLISIONS

Much of the information gained up to now is displayed pictorially in Fig. 24, which shows a central oxygen-lead collision just after the last interaction of the produced pions, in the centre of mass of the "fireball". The labels in Fig. 24 refer to the following points:

1. The dotted outline shows that the empty volume which would be occupied by the projectile: emulsion experiments which can measure down to very small angles find no projectile fragments when high E_T events are selected [32].

2. The region between the projectile and the fireball is observed to contain a pion flux consistent with leading quark hadronization or with a Landau expansion. Future particle composition studies may determine which description is more appropriate.

3. The black region shows the initial volume occupied by the deposited energy in the Landau model, determined by geometry in the full stopping case. This leads to energy density of order 10 GeV/fermi^3 if the equilibrium is indeed established, as we believe is probably indicated by the large increase in strange particle production. This will be ascertained by observation of thermal radiation of lepton pairs when experiments in the appropriate kinematic region are done.

4. The shaded region shows the spatial dimensions of the fireball at pion freezeout, as described in the previous section, Table 4.1.

5. The great stability of the pion mid-range p_T slope could indicate a latent heat is involved in the evolution of the deposited energy. Measurements of low p_T antiprotons to determine the radial flow are needed.

6. In the direction of the heavy target, additional protons are observed, removed from the outer regions of the collision volume in the target, shown to be missing, label (8).

7. The target fragments are observed in the 'plastic-ball' detector [33], which finds the target to be completely disrupted, indicating some mechanism of transferring the necessary energy, which is still a small fraction of the total E_T.

8. The time scale of pion emission is especially important: the first measurement reported in Table 4.1, indicates that the lifetime of the emission is order 12. fermi/c, long compared to the ordinary spatial scale of a few fermi/c in the direction of the effect predicted for a strong phase transition. It is important to strengthen this conclusion.

6. PROBING THE SPACE AROUND AN INTERACTION

The ideal version of such an experiment was described in the introduction: colour fields are generated in a hadronic interaction, and electromagnetic radiation is observed from the area outside the usual interaction volume, Fig. 3. Several experiments of this type have been performed, studying either real photons or virtual photons internally converting into a pair of leptons, starting some years ago with the observation of 'anomalous lepton pairs' occurring at low mass, at a surprising large rate [33]. Only more recently has it become clear that the spectrum of mass and p_T extended to such low values as to

exclude a phenomenon which originates inside the one or two fermi radius of a hadronic interaction [34]. This aspect has been much strengthened by observation of the copious production of the corresponding real photons with transverse momenta as low as 10 MeV or less [35].

The cross-sections for real and virtual photons may be compared by using the theory of soft internal conversion, used to display a compilation of photon and lepton pair data in Fig. 25, as a function of the transverse mass variable. We see a spectrum which rises steadily as m_T approaches zero, whereas it was generally supposed that such a phenomenon, of hadronic origin, should level-off at the hadronic scale of about 300 MeV.

There is an uninteresting source of radiation, inner bremsstrahlung, due to the radiation of charge by the outgoing particles created in the interaction. This radiation extends to very long wavelengths since the path of the outgoing particles in effectively infinite, leading to a spectrum proportional to $(E\gamma)^{-1}$, somewhat similar to the data, but, as shown in Fig. 25 the bremsstrahlung explains only a quarter or less of the data for $E\gamma$ above 10 MeV [37].

The excess becomes much greater when one selects only events with a high number of charged tracks. Note that the net charge of the particles created in the collision is zero, so that the radiation is due to fluctuations in the number of charged particles in a given solid angle. The radiation varies as the square of the net charge in the relevant solid angle; the mean net charge varies as the square root of the number of charged particles; and thus it is found that the number of photons varies linearly with the number of charged particles. The ratio of the number of photons in a given energy range to the number of charged particles in the same solid angle is a number which can be calculated rather precisely, small effects due to measured particle correlations can be included, and it is found that the result is approximately the same for different reactions and incident (high) energies.

The data, presented in Fig. 26 for real photon to pion ratios as a function of multiplicity of charged particles [38], present a very different picture, with an approximately linear variation which corresponds to a quadratic dependence of photon radiation on particle number. Such a dependence (seen also in the virtual photons) is characteristic of radiation from charge confined in a volume, and this is believed to be such a case, but then the long wavelength of the observed radiation implies that the volume of the box is very large, on a hadronic scale.

The most straight-forward, but unexpected, explanation is that given by Van Hove [39], who invokes the existence of a cold gas of very low energy quarks and gluons filling a large volume. This accounts for the radiation we are discussing as well as some related effects in high multiplicity pion emission, but such a state of matter is a surprising phenomenon. Since it involves a large number of very low energy particles, it is characteristic of an attempt to describe microscopic fields by particles, and may then represent a point of contact with the attempts to observe the colour vacuum polarization described in the introduction.

One tries hard to find more mundane sources for the radiation. It is true that decaying resonances, ρ, ω^o and so on, fill a large volume, similar to that required, but radiation from their charged decay particles has already been included in the calculation of inner bremsstrahlung, ignoring interference between the different sources of radiation. This approximation should be checked.

Clearly further experimental and theoretical investigations of this radiation are eagerly awaited.

REFERENCES

[1] E.V. Shuryak, the QCD vacuum, Hadrons and the Superdense Matter; (World Scientific, Singapore, 1988).

[2] C. Alcock, Ann. Rev. Nucl. Particle Phys. 38 91988) and Cosmological Consequences of the Quark-Hadron Phase Transition, plenary talk at "Quark Matter '88", Lenox, Mass. 1988 (to be published).

[3] See "Quark Matter '87", Z. Phys. C38 (1988).

[4] F. Karsch, in Ref. 3, p. 147.

[5] J.E. Elias et al., Phys. Rev. D22, 139 (1980);
K. Braune et al. Z. Phys. C17 (1983) 105-112.

[6] E. Fermi, Prog. Theor. Phys. 5, 570 (1950); Phys. Rev. 81, 683 (1951).

[7] E.V. Shuryak, Phys. Lett. B78, 150 (1978); J.D.Bjorken, Phys. Rev. D27, 140 (1983).

[8] L.D. Landau, in Collected papers of L.D. Landau, ed. D. Ter Haar (Gordon and Breach, New York, 1965); P. Carruthers and Minh Duong/van, Phys. Rev. D8, 859 (1973).

[9] W. Busza and A.S. Goldhaber, Phys. Lett. B139, 235 (1983).

[10] T. Åkesson, Z. Phys. C38, 397 (1988).

[11] T. Åkesson et al., Z. Phys. C38, 383 (1988)

[12] T. Åkesson et al., as quoted in [16] and submitted to Phys. lett. B.

[13] P. Braun-Munzinger and J. Stachel, Phys. Lett. 216, 1 (1989).

[14] B. Alpher et al., Nucl. Phys B100, 237 (1975);
K. Güttler et al., Phys. Lett. 64B, 111 (1976).

[15] P.J. Siemens and J.O. Rasmussen, Phys. Rev. lett. 42, 880 (1979).

[16] J. Schukraft, CERN-EP/88-176 (1988) (to appear in "Quark Matter '88).

[17] J.W. Cronin et al., Phys. Review D. 11, 3105 (1975).

[18] J.W. Harris, in "Quark Matter '88";
K.S. Lee and U. Heinz, Regenslung preprint TPR-88-16, submitted to Z. Phys. C., and
U. Heinz, TPR-88-33.

[19] E.V. Shuryak, Phys. Lett. B207, 345 (1988).

[20] B.L. Fridman, GSI-88-65, to appear in "Quark Matter '88".

[21] P. Vincent, E-802, Results in "Quark Matter '88".

[22] M. Jacob, CERN PRE 88-071, Summary Talk to appear in "Hadron '88: Hadronic Matter in Collision, Tucson, Arizona 1988.

[23] R. Hanbury/Brown and R.Q. Twin, Phil. Mag. 45, 663 (1954).

[24] G. Goldhaber, S. Goldhaber, W. Lee and A. Pais, Phys. Rev. 120, 300 (1960).

[25] G. Gyulassy, S.K. Kaufman and L.W. Wilson, Phys. Rev. C20, 2267 (1979).

[26] G.I. Kopylov and M.I. Podgoretsky, Sov. J. of Nuclear Phys. 18, 336 (1974).

[27] T. Müller, Proc. XIV Int. Symp. on Multiparticle dynamics, World Scientific, Singapore 1984, p.528.

[28] T. Åkesson et al., Z. Phys. C36, 517 (1987).

[29] S. Pratt, Phys. Rev. D33, 1314 (1986);
A. Makhlin and Y. Sinykov, Kiev preprint ITP-87-645 (1987);
G. Bertsch, M. Gong, M. Tohyama, Phys. Rev. C37, 1986 (1988).

[30] A. Bamberger et al., Phys. Lett. B203, 320 (1988), and Ref. [17].

[31] M. Gyulassy and S.S. Padula, LBL-26077 (1988). To appear in Phys. Rev. Letters.

[32] G. Romano, Summary of emulsion results, in "Quark Matter '88".

[33] K.J. Anderson et al., Phys. Rev. lett. 37, 799 (1976).

[34] T. Åkesson et al., Phys. Lett. 192B, 463 (1987);
V. Hedberg, Thesis, Univ. Lund, LUNFD6 (NFFL-8037) (1987).

[35] P.V. Chliapnikov et al., Phys. Lett. B141, 276 [1981].

[36] W.J. Willis, PANIC Conference Kyoto, Japan (1987);
U. Goerlach, Lepton-Photon Conference, Munich (1988);
A. Pfeiffer, Thesis, Univ. Heidelberg, (1988).

[37] R. Ruckl, Phys. Lett. 64B, 39 (1976).

[38] See Ref. [36] and HELIOS Collaboration "Direct Soft Photons in 450 GeV/c p-Be and p-Al collisions" to be published.

[39] L. Van Hove, CERN-TH. 5236/88, to appear in Ann. Physics.

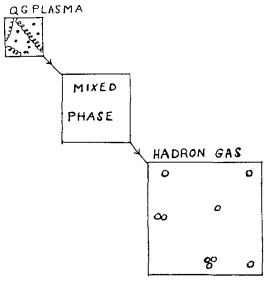

Fig. 1 Schematic drawings of the three states passed through successively, starting with very high energy density.

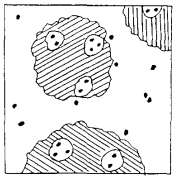

Fig. 2 Arbitrary assumptions have been used to create a speculative drawing of the mixed state at a point midway in its expansion. The shaded region denotes physical vacuum in which coloured particles are confined. The remainder is the perturbative vacuum.

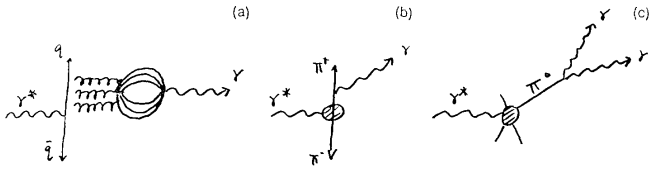

Fig. 3 (a) Schematic illustration of a hypothetical soft colour excitation of the physical vacuum.
(b) The trivial background to (a) coming from inner bremsstrahlung of the charged particles produced.
(c) The still more trivial background of photons (and soft lepton pairs) from meson decay.

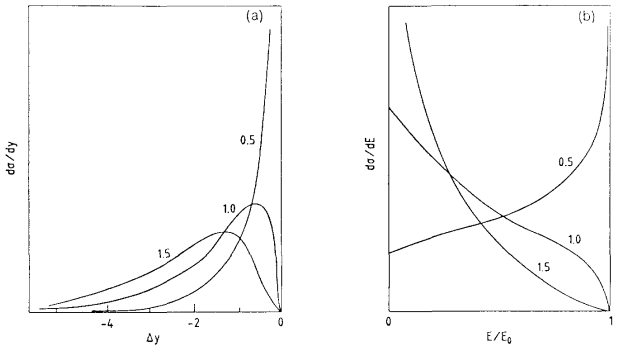

Fig. 4 (a) The energy spectrum of an electron after traversing 0.5, 1.0 and 1.5 radiation lengths of matter. (b) The same spectra but in terms of rapidity shift from the incident electron.

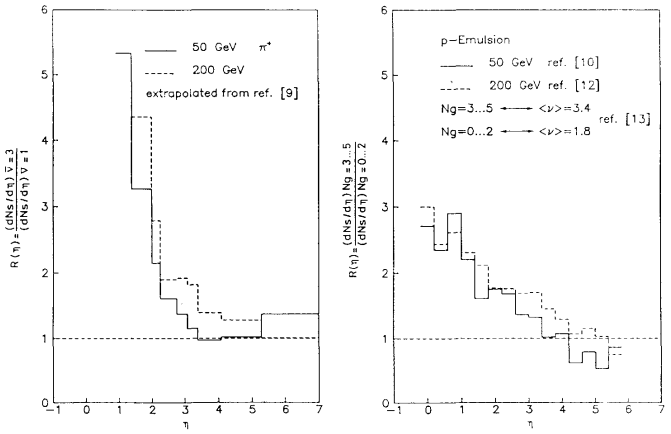

Fig. 5 The ratio of the pseudorapidity distributions of charged particle production for "lead" and hydrogen targets, showing that the multiplicity does not change for h ≥ 3, the forward hemisphere in the centre-of-mass system. The data are from Elias et al. and several emulsion experiments as analysed by Braune et al. [5].

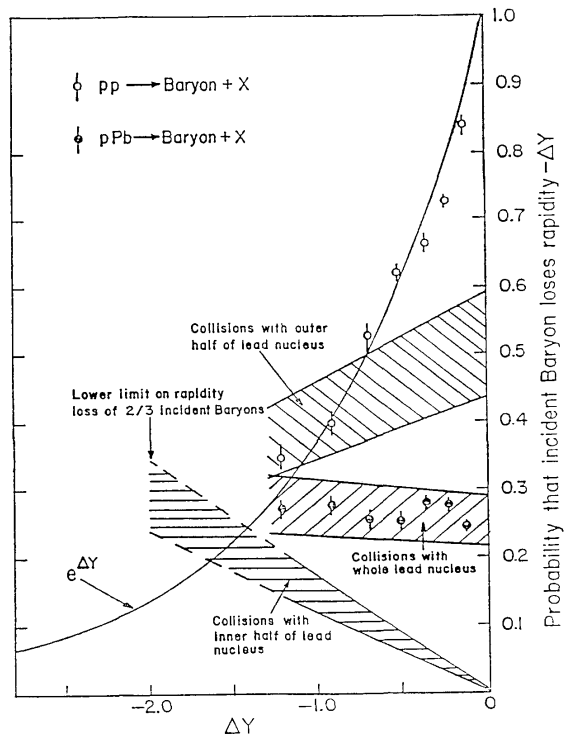

Fig. 6 Probability distributions to lose rapidity -Δy in collisions with protons or lead nuclei, and approximate estimates of the distributions of collisions with lead in particular impact parameter ranges from Busza and Goldhaber [9].

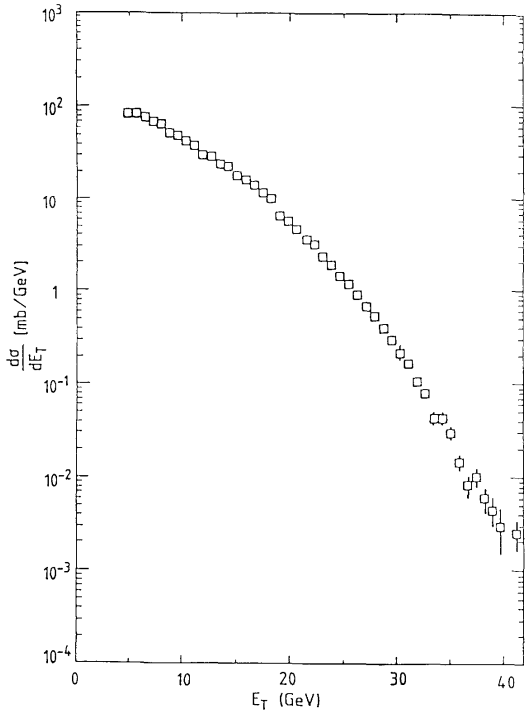

Fig. 7 The distribution in transverse energy for 200 GeV proton-lead collisions [16].

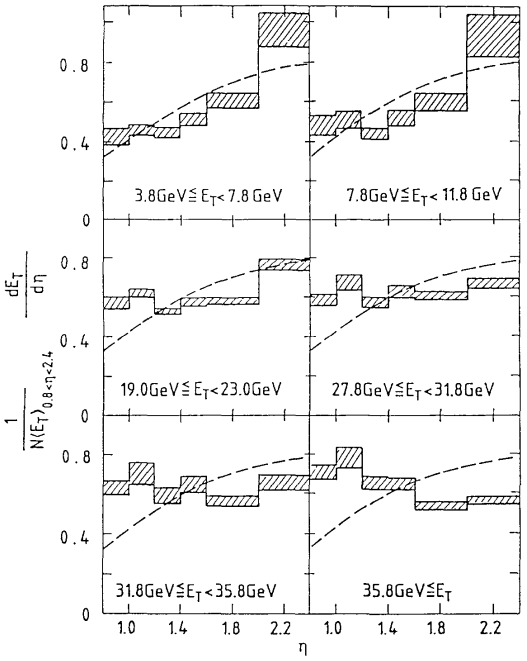

Fig. 8 The distribution of transverse energy in pseudorapidity for various E_T values, for 200 GeV proton lead collisions [10].

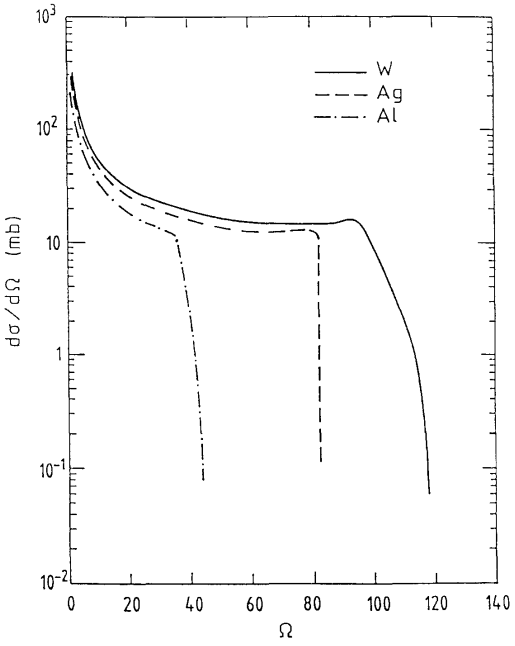

Fig. 9 Geometrical cross-section as a function of the value of the number of collisions $N = \sigma_{pp}\Omega$, where Ω is the overlap integral $\int_{p1} \times_{p2} dS$, for oxygen collisions with Al, Ag, and W nuclei [11].

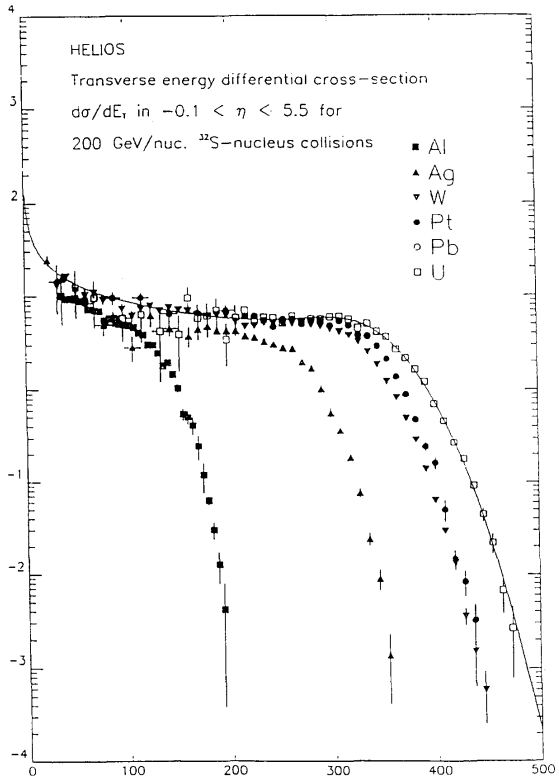

Fig. 10 Cross-section as a function of transverse energy in the interval $-0.1 < \eta < 5$ for 200 GeV/nucleon sulphur collisions with different targets [12].

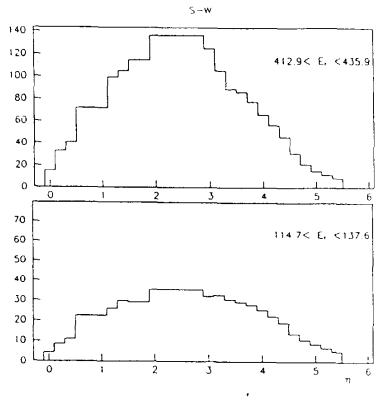

Fig. 11 The distribution of E_T in pseudorapidity for two values of E_T, for 200 GeV/nucleon sulphur-W collisions [12]. The smaller value of E_T is in the "plateau" region of the E_T distribution while the larger value is in the tail of the distribution for central collisions.

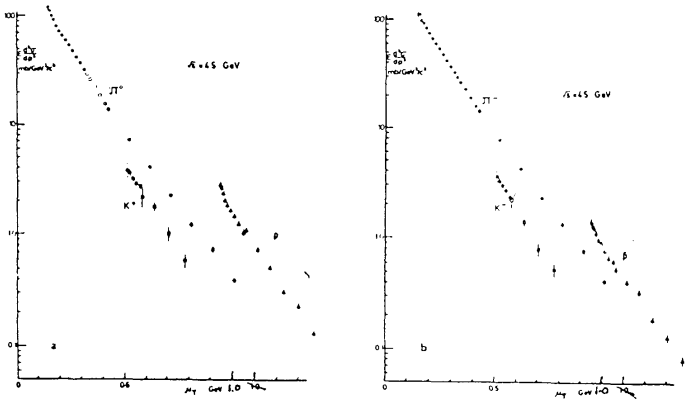

Fig. 12 Differential cross-sections as a function of m_T for proton-proton collisions at the ISR [14]. In the centre-of-mass, the charged particles are measured at 90° to the beams, and the energy is 45 GeV/c.

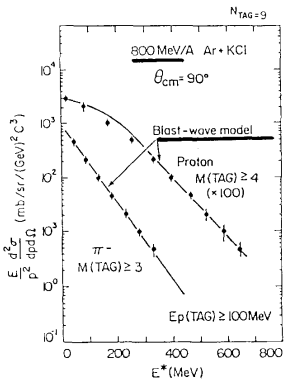

Fig. 13 Differential cross-sections as a function of kinetic energy in the centre-of-mass (equal to m_T within an additive factor and consequently suitable for comparison with the previous Figure [15]). The reaction is 800 MeV/nucleon (laboratory energy) ^{20}Ne on NaF. The curves are a fit to an expanding fireball.

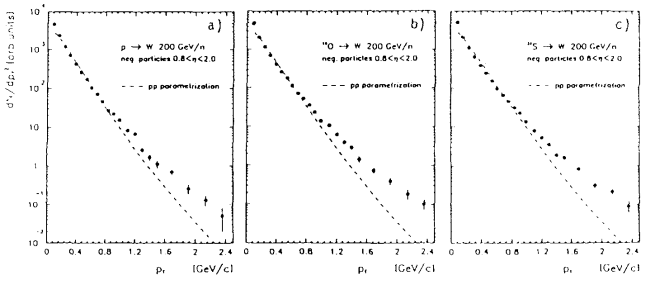

Fig. 14 Cross-section dN/dp_T^2 of negative particles in the region $0.8 < z < 2.0$ for (a) p-W, (b) ^{16}O-W, (c) ^{32}S-W reactions at 200 GeV/n [16]. The dashed lines are arbitrarily normalized parametrizations of pp data.

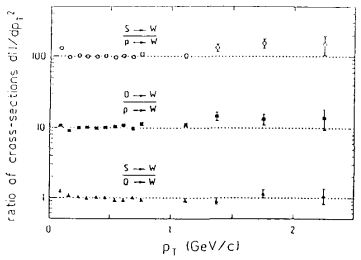

Fig. 15 Ratio of the cross-sections dN/dp_T^2 as a function of pT for negative particles in the region 0.8 < y < 2.0 [16]. Upper part: S-W divided by p-W. Middle part: O-W divided by p-W. Lower part: S.W. divided by O-W. The relative normalization is arbitrary.

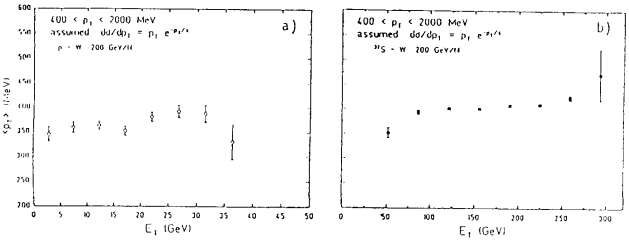

Fig. 16 E_T dependence of the average transverse momentum of negative particles in (a) p-W and (b) ^{32}S-W reactions, extracted from the slope of an exponential distribution fitted to the data in the region 400 < p_T < 2000 MeV/c [16].

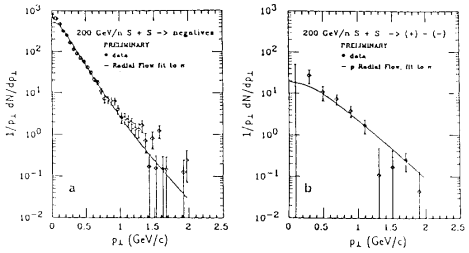

Fig. 17 Results from the Streamer Chamber for transverse momentum distributions for central collisions of 200 GeV/n S + S for a) negatively-charged particles (2 < z < 3) and b) the difference of positively- and negatively-charged particles assuming they are protons, together with a fit to both spectra with a model assuming a radial motion of a thermal system [18].

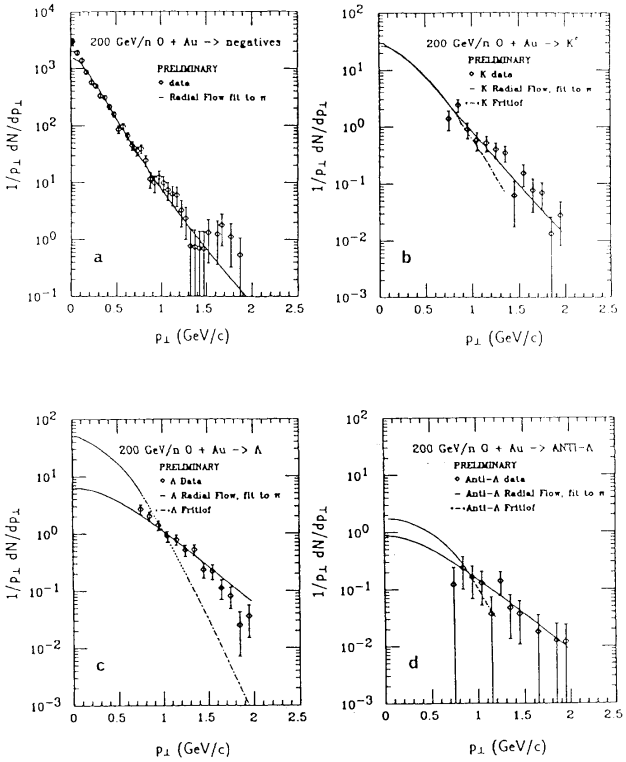

Fig. 18 Streamer chamber results for transverse momentum distributions for central collisions of 200 GeV/n O+Au for the particles indicated on the figures [18]. Also shown are predictions of a radial expansion model (solid curve) fitted to the distribution of negatives in a) and the Lund/Fritiof model (dot-dash curve), intended to represent the shape of the data in nucleon-nucleon collisions.

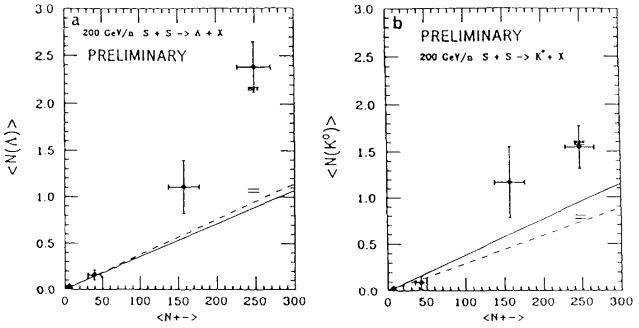

Fig. 19 For 200 GeV/n S+S interactions, streamer chamber observations of the mean multiplicities of a) Λ's and b) K^0's as a function of the mean charged particle multiplicity in each event sample [18]. the solid lines are predictions of the Lund/Fritiof model and the dashed lines those of an independent nucleon-nucleon model. The double line is the prediction of a hadron gas model for central collisions and the triple line that for a parton gas.

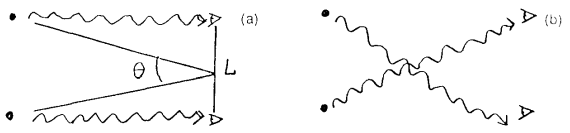

Fig. 20 Diagram defining the geometry for two-photon interference and showing the two states (a) and (b), which must appear in a symmetrical wave fun ction.

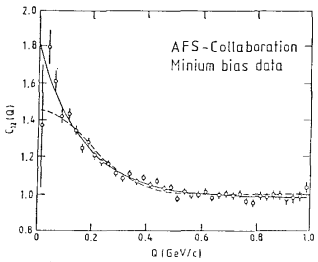

Fig. 21 The two-pion correlation function for pions in the central region of proton-proton collisions at 63 GeV in the centre of mass [28].

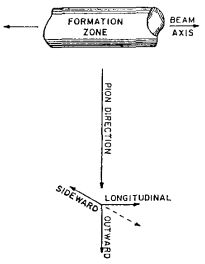

Fig. 22
A suitable coordinate system for measuring two-pion correlations produced by relativistic particles, which are along the vertical direction in the picture. The rest-frame of the figure is such that the first pion is at 90° to the beam, and the second pion is analysed along the three axes indicated.

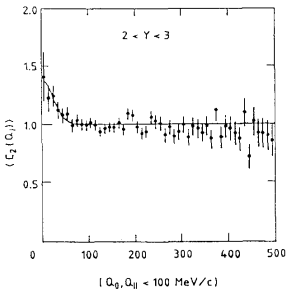

Fig. 23 An example of the correlation measured for two negative particles in oxygen-gold collisions at 200 GeV/nucleon, showing the enhancement low values of the Q-value of the two charged particles [30].

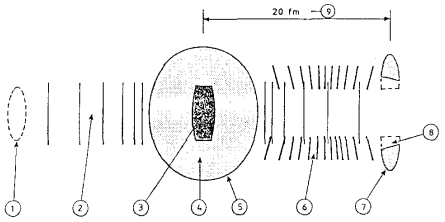

Fig. 24 A pictorial summary of the results of the 200 GeV per nucleon experiments to date, as interpreted in terms of a space-time snapshot at the time of pion freeze-out. A key in the text explains and justifies the numbered features.

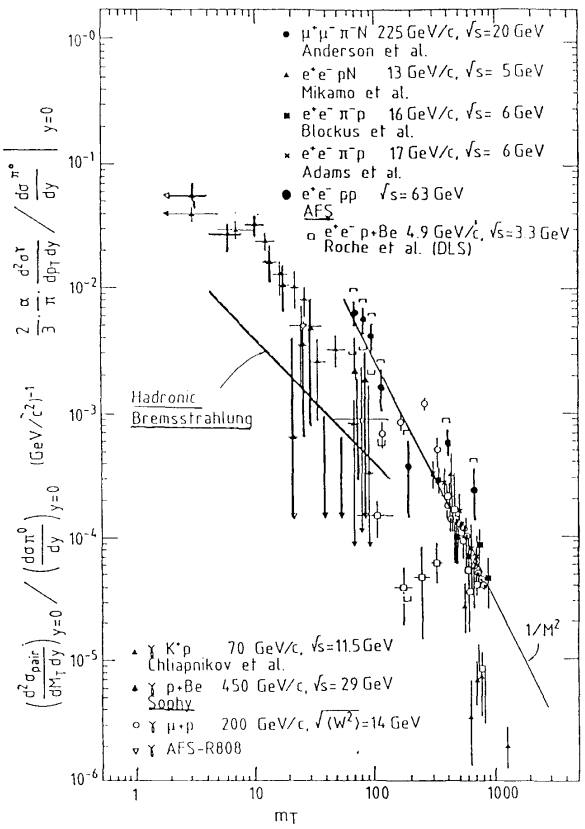

Fig. 25 A compilation of data on soft photon and virtual photon production at different energies and by different particles, displayed as a function of the m_T of the photon or pair. The formula for internal conversion has been used to display real and virtual photons together. Also shown is the production for the background process of inner bremsstrahlung which has not been subtracted [36].

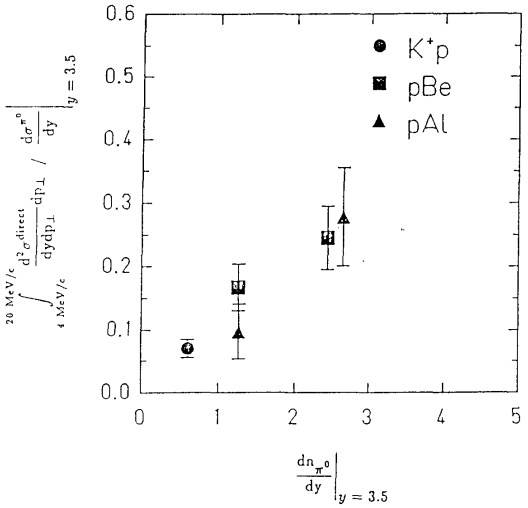

Fig. 26 The ratio of photons production to pion production as a function of the number of charged particles is shown for data for different particles and beams. Inner bremsstrahlung would give a constant of this plot [36].